JACS Au
AN OPEN ACCESS JOURNAL OF THE AMERICAN CHEMICAL SOCIETY

pubs.acs.org/jacsau Letter

Two GPSes in a Ball: Deciphering the Endosomal Tug-of-War Using Plasmonic Dark-Field STORM

Siwoo Jin, Jiseong Park, Wonhee John Lee, Yongdeok Ahn, Youngchan Park, Minsoo Park, Inchan Hwang, Kwanyong Seo, and Daeha Seo*

Cite This: *JACS Au* 2022, 2, 1596–1603 Read Online

ACCESS | Metrics & More | Article Recommendations | Supporting Information

ABSTRACT: Live video recording of intracellular material transport is a promising means of deciphering the fascinating underlying mechanisms driving life at the molecular level. Such technology holds the key to realizing real-time observation at appropriate resolutions in three-dimensional (3D) space within living cells. Here, we report an optical microscopic method for probing endosomal dynamics with proper spatiotemporal resolution within 3D space in live cells: plasmonic dark-field STORM (pdf-STORM). We first confirmed that pdf-STORM has a spatial resolution comparable to that of scanning electron microscopy. Additionally, by observing two optical probes within a single organelle, we were able to track rotational movements and demonstrate the feasibility of using pdf-STORM to observe the angular displacements of an endosome during a "tug-of-war" over an extended period. Finally, we show various biophysical parameters of the hitherto unelucidated dynamics of endosomes—angular displacement is discontinuous and *y*-axis movement predominates and follows a long-tail distribution.

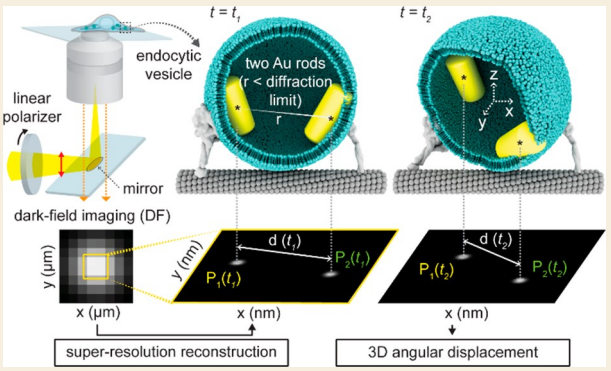

KEYWORDS: *plasmonics, dark-field microscopy, super-resolution imaging, bioimaging, intracellular transport, three-dimensional rotation, endosomal tug-of-war*

Material and signal transports in living cells comprise sequences of intricately organized movements in crowded three-dimensional space and time. These dynamics are reversible, and the equilibrium between active and passive processes is vital for signal transduction.[1] Anomalous movements are implicated in neural,[2,3] muscular,[4] and vascular disease.[5] Therefore, probing endosomal dynamics with a proper spatiotemporal resolution and observed duration is key to understanding not only endosomal transport mechanisms, which are frequently described as a "tug-of-war", but also impaired metabolism in related diseases.[6] Fluorescence microscopes that can overcome the diffraction barrier have enabled the direct observation of subcellular organelles even at a single-molecule level,[7] and recently, the introduction of inorganic nanoparticles, e.g., plasmonic nanoparticles, allows for imaging of angular displacements in 3D space as well as long-term observation.[8−10] However, precise tracking in live cells over an extended period requires imaging techniques that offer geometric sensitivity and higher optical stability. Here, we demonstrate a novel form of long-lasting super-resolution dark-field microscopy, called "pdf-stochastic optical reconstruction microscopy" (pdf-STORM) in live cells, which can accurately determine the positions and orientations of an endosome in real time. A key principle of distinguishing objects within the diffraction limit (usually ∼200 nm in a conventional microscope) in super-resolution (SR) techniques is the visualization of reversible transitions of fluorescence between the "on" and "off" states.[11,12] For example, recently developed protocols such as stimulated emission depletion microscopy (STED) and stochastic optical reconstruction microscopy (STORM) use instrumentally controlled and spontaneous switching of fluorophores, respectively, to resolve neighboring molecules. For optical switching in dark-field (DF) microscopes, we used gold nanorods (AuNRs) as the blinking probes and constructed an epi-polarization DF microscope[10] using a rotating linear polarizer and dot mirror (Figure 1a and Figure S1). Due to the polarization-angle (θ_{pol})-dependent intensity of the linear plasmonic nanoparticle (I_{NR}, Figure S2),[13] continuously changing θ_{pol} can generate reduplicative blinking and resolve the randomly oriented NRs within the diffraction limit using the STORM algorithm (Figure S3a−d).

Received: March 19, 2022
Revised: May 16, 2022
Accepted: May 17, 2022
Published: May 19, 2022

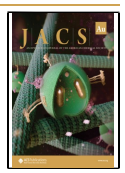

https://doi.org/10.1021/jacsau.2c00180
JACS Au 2022, 2, 1596−1603

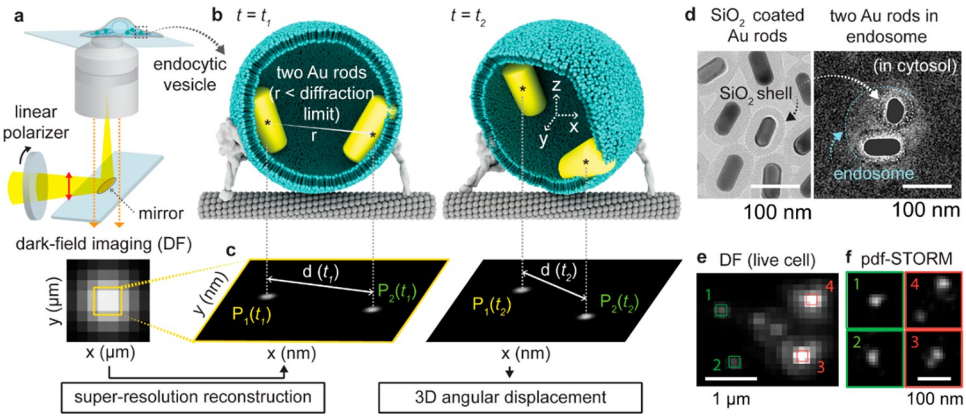

Figure 1. Schematic illustration of the pdf-STORM for observing the angular displacement of endocytic vesicles in live cells. (a–c) Experimental scheme for pdf-STORM. (a) Diagram of the microscope setup for dark-field imaging with polarized excitation. Linearly polarized light is reflected from the dot mirror through the objective (100×, 1.49 NA) onto the cell; the light scattered by the plasmonic nanoparticles was visualized with an electron-multiplying charge-coupled device (EM-CCD) in epi-mode configuration. (b) Schematic illustration showing the angular displacement of endosomes. (c) Movements of endosomes containing two optical probes. AuNRs within the diffraction limit can be monitored by super-resolution reconstruction. The 2D projected coordinates for the resolved AuNRs over time ($P(t)$) can be analyzed by rotation in 3D space. (d) Transmission electron microscopy images of the rods in an early-stage endosome. Since the AuNRs are coated with a SiO_2 and Tf shell and the endosomes appear to contain two NRs bound tightly in the early stage of internalization, the AuNRs can be seen on both ends of the endosome without optical coupling. (e, f) Observation of endosomes in live cells. (e) Dark-field images of endosomes acquired after cellular uptake without the polarizer in live cells. (f) Resolved pdf-STORM results of the small region marked with a colored box and numbered in (e). Spots with brighter scattering signals (3, 4) are divided into two separate signals, whereas the dim spots (1, 2) are not.

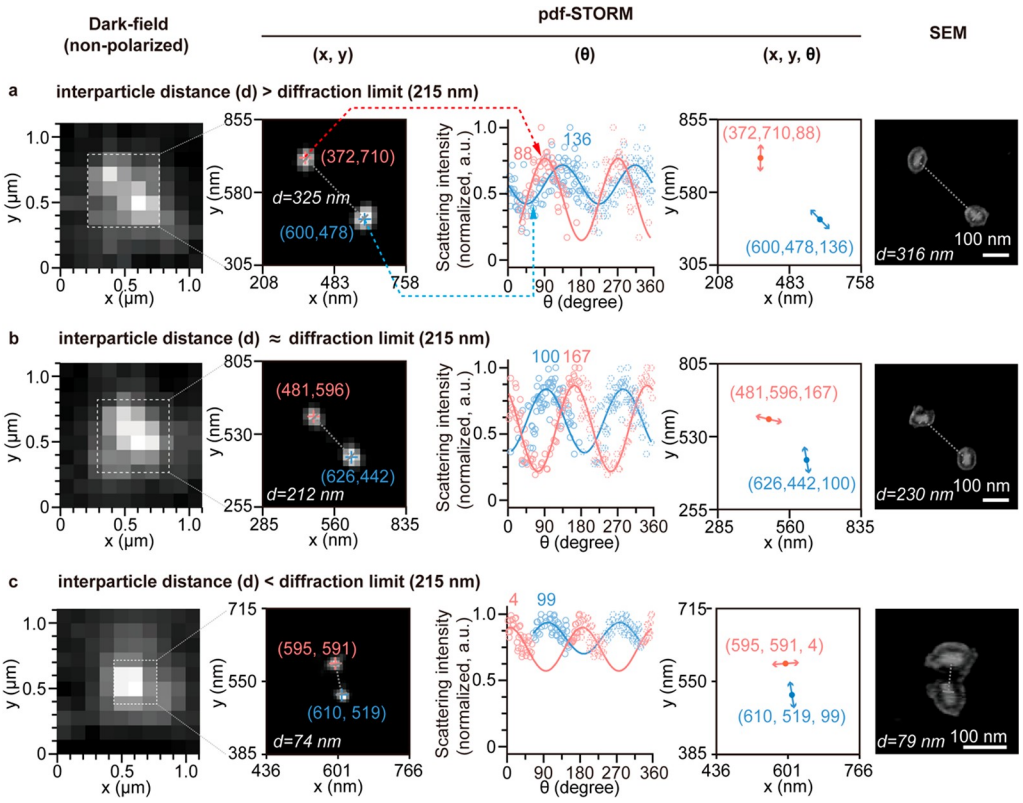

Figure 2. The performance of pdf-STORM is comparable to that of electron microscopy on a 2D plane. Conventional dark-field (DF) images (left column, without polarizer, DF) are reconstructed to form super-resolution images (middle columns) containing the orientation information on each AuNR probe (θ) and information on coordinates (x, y). The diffraction limit of the optical setup is defined as 215 nm (according to Abbe's law, $\lambda/2NA$, where, λ and NA denote the wavelength of light and numerical aperture of the objective lens, respectively). Three representative pdf-STORM results depending on interparticle distance are shown: (a) interparticle distance > diffraction limit, (b) interparticle distance ≈ diffraction limit, and (c) interparticle distance < diffraction limit. Combining the location information (middle-1, (x, y)) from pdf-STORM forms a white box in the DF with angular information (middle-2, θ). A spatioangular map of each AuNR was reconstructed (middle-3) and compared with those obtained using scanning electron microscopy (SEM, right column). AuNRs were spatially well resolved, and the orientation of AuNRs matched the findings of SEM analysis well. In comparison with SEM, pdf-STORM shows differences of <10%.

https://doi.org/10.1021/jacsau.2c00180
JACS Au 2022, 2, 1596–1603

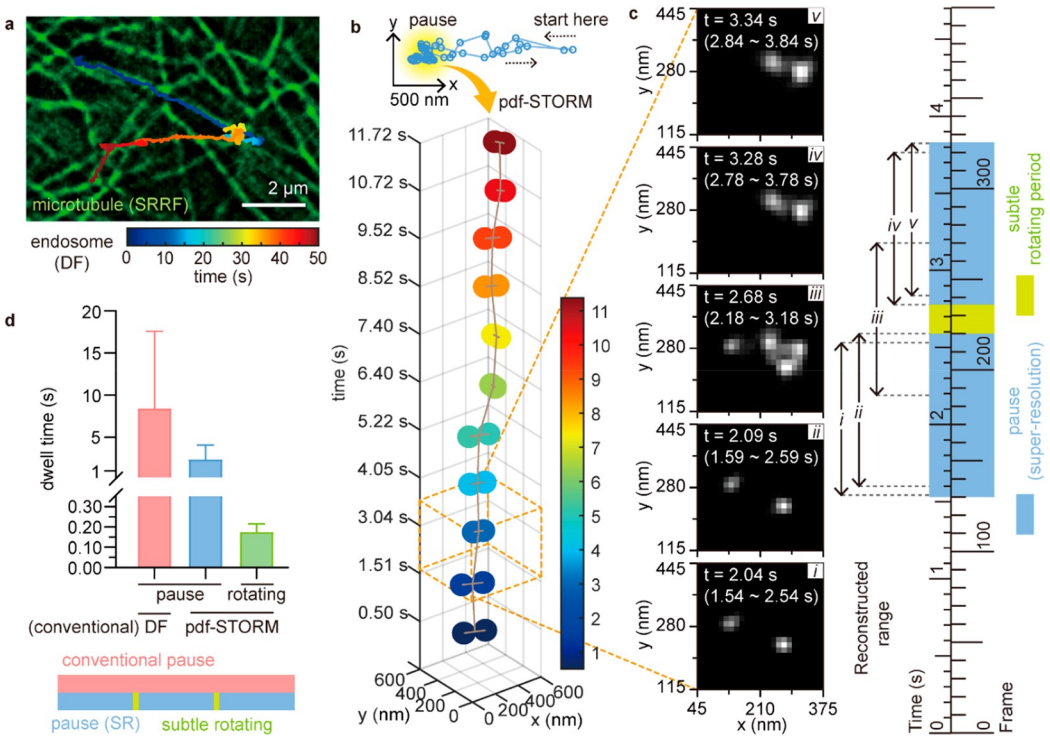

Figure 3. Discontinuous and rapid angular displacement of an endosome at a crossroad of microtubules during a conventional pause. (a) Endosomal transport on a microtubule (MT) network. The trajectories of the endocytic vesicle (in conventional DF) are color-coded to show the traveling time and were overlaid on MT networks (super-resolution radial fluctuation, SRRF). In many observations, all stoppages of endosomes occurred at intersections of MTs. (b) Representative pdf-STORM trajectory (2D-projected images for ~11 s) of a single endosome (two AuNRs) at the pause state. The (x, y) coordinates and the interparticle distance $(d(t))$ of each NR changed irregularly within the diffraction limit. (c) Typical single rotational motion, occurring over approximately 2.7 s. The movement indicated by the orange dotted box in (b) was analyzed in detail. Here, a single pdf-STORM image was acquired from ~85 frames (~1 s) of polarized DF images, and the reconstructions were made continuously while sliding the frames one by one (i–v are their representative results). Images in intervals of i–ii and iv–v show that the endosome does not move, and the four well-separated spots in iii, which have positions identical with those in ii and iv, indicated that there is a discontinuous and rapid displacement in the reconstruction period, especially in the region marked in green on the time axis (right, rotating period). (d) Statistical analysis of dwell time for conventional pause, super-resolution pause states, and rotating periods between the super-resolution pauses (8.5 ± 9.2, 2.5 ± 1.6, and 0.17 ± 0.04 s, respectively).

We performed an extended observation of the endosome containing the two AuNRs using pdf-STORM. We inferred endosomal rotation, e.g., Eulerian angles, from the sequence of projected images (Figure 1b,c). The ideal geometric probe for the angular displacement of intercellular objects would have (i) at least two θ_{pol}-sensitive AuNRs for SR reconstruction, (ii) an insulating layer that prevents coupling of optical properties,[14] i.e., plasmonic coupling, by maintaining their distance, (iii) multiple binding molecules that prevent the random motion of the tethered probes by immobilizing them inside the vesicle. Therefore, the AuNRs were sequentially coated with silicon dioxide (SiO_2)[15] using the Stöber method and conjugated with transferrin (Tf), an excess endocytosis-triggering protein, through an electrostatic interaction (Figure S4a–f). We selected the brighter spots that had two AuNRs in DF microscopy. The resulting characterization of AuNRs and their observation within a live cell by DF provided direct evidence that probes are specifically internalized (Tf-mediated endocytosis) while maintaining colloidal stability (Figure S4)[16] without random tethered motion (Figure S5) that perturbs the analysis of endosomal movements, due to the optical coupling and the Brownian motion of the probe. Additionally, we performed transmission electron microscopy (TEM) on a section of two-dimensional cultured whole cells. The corresponding TEM image of the early-stage endosomes also supports the notion that Tf-coated NRs were indeed endocytosed, immobilized on the inner surface of the endosome, and tightly covered with a endosomal membrane and were not in direct contact with NRs—due to their SiO_2 shell (Figure 1d).

Given the proper colloidal and optical conditions of the probes and the polarization of the DF microscope, we first investigated whether pdf-STORM can separate component probes in the cytosolic area by bright scattering (Figure 1e,f). The resulting reconstructed images clearly resolve brighter spots for each probe, while the dim scatterings assumed to be a single NR do not. We next performed additional microscopic evaluation with virtual experiments using synthetic data (Figure S6 and Movie S1). The scattering signal of a single AuNR in polarized DF depends on the plasmonic length,[17] the length over which surface electron oscillations take place, which can be changed by θ_{pol}. We generated a θ_{pol}-dependent synthetic sequence of images that replicate the spot size and intensity obtained from DF images of a single AuNR. We placed the two NRs at various vertical distances within the diffraction limit and reconstructed them using the STORM algorithm,[18] confirming that they were successfully resolved. These results demonstrated the potential of pdf-STORM to observe the micromovements of the endosome.

https://doi.org/10.1021/jacsau.2c00180
JACS Au 2022, 2, 1596–1603

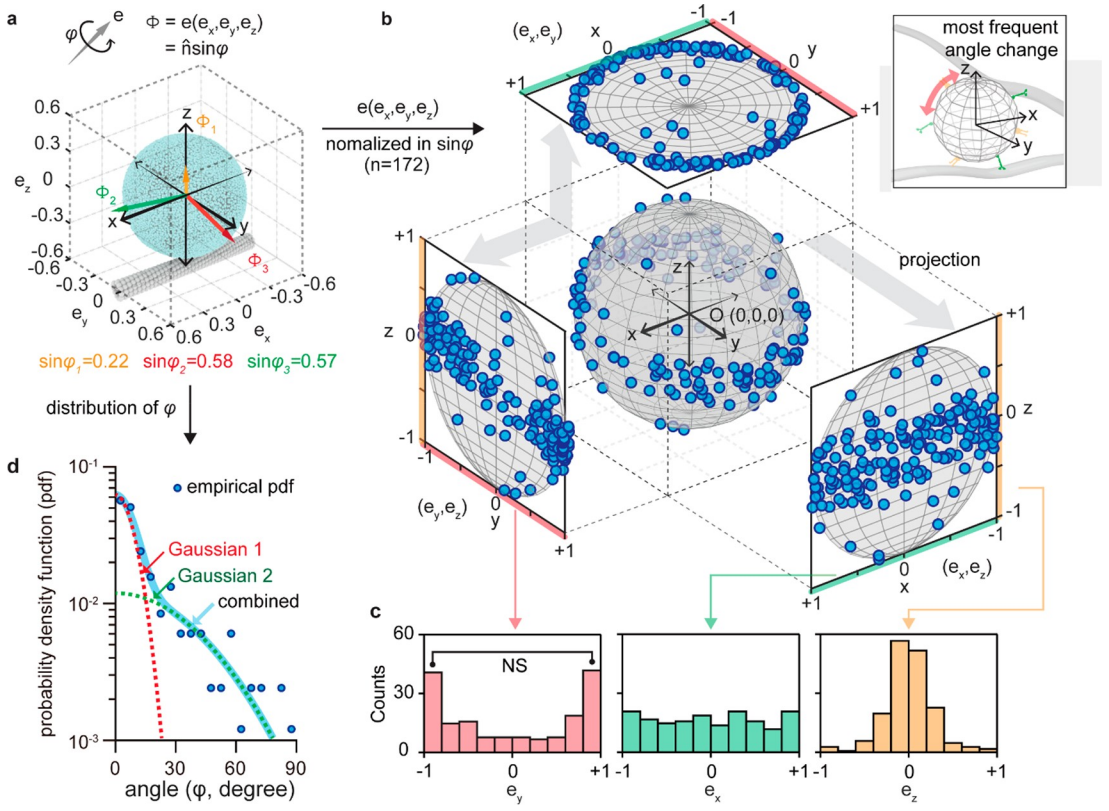

Figure 4. The preferred rotation axis of endosomes in 3D space and the angular size distribution. (a) Representative Euler vectors of endosomal rotation ($\Phi = \hat{n}\sin\varphi$, where $\hat{n}$ is the unit vector representing the direction of the axis and φ is the angle). The rotating axis is derived through the long-term observation of $d(t)$ and the position of the AuNRs in the endosome (see Note S2 for a detailed description). (b) Statistical analysis of the direction of the rotational axis (normalized in sin φ) and the projection on the 2D planes. (c) Histogram of each component of Cartesian coordinates for the normalized rotation axis. On the basis of the analysis (b, c), 3D angular displacement is mainly distributed in the equatorial direction and is y axis dominant, indicating that endosomes tend to roll to existing microtubules at pause (inset on upper right). (d) Probability density function (pdf) for the distribution of φ. The two combined Gaussian distribution models were the best fit to explain pdf (see Figure S14 for a comparison).

We also performed proof of concept experiments to confirm the reliability and validity of pdf-STORM, by observing randomly oriented NRs (Figure 2). AuNRs were immobilized such that they did not wobble, the SiO_2-coated NRs were bound nonspecifically and sparsely on the glass surface, the coverslips were dried in air, and then the same NRs were imaged with both pdf-STORM and scanning electron microscopy (SEM). We first obtained a sequence of DF stacks of spots while changing the θ_{pol} (Figure 2, dark field), and they were reconstructed as an SR image using the STORM algorithm (Figure 2 (x, y)). The intensity of each separated position was postmeasured as a function of θ_{pol} and fitted to the sine curve, and the maximized angle was read as the orientation of each NR (θ_{NR}). The resulting coordinates (x, y, θ_{NR}) of each NR were well matched with those obtained in SEM analysis, and this observation held similarly for all cases irrespective of interparticle distances and relative angles (Figure 2 (x, y, θ_{NR})) and SEM (Figure S7). They ensure that plasmonic signals from adjoining probes within the Abbe diffraction limit (~250 nm, $d = \lambda/2NA$) could be spatially resolved and that the orientation of NRs was measured with accuracy comparable to that of SEM. Second, as a negative control, we performed a pdf-STORM analysis when (i) NRs were aligned parallel so that two I_{NR} values were synchronized in time (Figure S8a), (ii) the interparticle distance is short enough to bring out the plasmon coupling (without the SiO_2 shell, Figure S8b), and (iii) probes were θ_{pol}-insensitive, e.g., Au spheres (Figure S9).

Third, as a positive control, we applied pdf-STORM to resolve randomly moving tethered NRs under fixed polarization to confirm whether our SR is indeed from the plasmonic length change (Figure S3e–g). We prepared monovalently conjugated NRs (mNRs) with a flexible linker that allows biotin functionalization,[19,20] immobilized them onto the streptavidin surface (Figure S10), and successfully reconstructed an SR image (Figure S11). Additional experiments using pdf-STORM with randomly blinking DF signals also revealed that our SR techniques could resolve neighboring spots with negligible error (Figure S6c and Movie S2). We therefore conclude that the key principle of our SR imaging is a reversible transition of the plasmonic signal depending on polarization and that both instrumentally controlled (rotating polarizer) and spontaneous blinking (Brownian motion of mNRs) are appropriate for SR reconstruction.

Intracellular vesicles are transported bidirectionally due to the coexistence of motor proteins, i.e. kinesin and dynein, which simultaneously move cargo in opposite directions along a microtubule (MT).[6,21,22] To interpret this tug of war, several classes of models have been proposed to explain how bidirectional transport and pause are regulated: (i) the draw model, wherein the antagonistic motors are pulling with the same amount of force in the opposite direction, (ii) the

https://doi.org/10.1021/jacsau.2c00180
JACS Au 2022, 2, 1596−1603

roadblock model, wherein obstacles in the crowded cellular environment disturb the movements, and (iii) the diffusive model, wherein all motors are detached from the MT or endosome. To visualize the endosomal transport on the MTs, we generated epithelial cells stably expressing tubulin-GFP as a model cell line and imaged the MT network using an SR fluorescence microscope (super-resolution radial fluctuations, SRRF) (Figure 3a). We successfully tracked the endosome simultaneously. Long-term observation of the endosomes using AuNR and DF microscopy revealed a sequence of antagonistic directional walking, with a velocity of 0.77(±0.40) μm/s and pausing with 8.5(±9.2) s of dwell time, as previously observed by conventional microscopy.[23] In addition, almost all observed pauses were only at the intersection of MTs, while the converse was not always true. This may be due to the lack of vertical contact between MTs or evasive maneuvers of the vesicles (Figure S12). This is consistent with the roadblock model of 1D-MT; however, long-term observation with high spatiotemporal resolution is needed for a further understanding of how the direction of material transport is determined in live cells. To address how the transport directions or endosomal orientations can be controlled efficiently in the maze of the intracellular network, we selected endosomes with brighter scattering intensities having two AuNRs at random (∼10% of the total spot under our endocytosis condition, Figure 1e,f) and conducted a time-lapse experiment using pdf-STORM to elucidate the endosomal rotational dynamics at the pause state (Figure 3b). In contrast to conventional SR techniques, the pdf-STORM of single endosomes marked with nonbleaching probes revealed the angular displacements of individual endosomes over a long period.

At the pause state, the position changes of NRs over time appeared to be discontinuous, on the basis of a pdf-STORM series (Figure 3c and Movie S3). This is because one pdf-STORM image was reconstructed out of ∼100 stacks ($\Delta\theta$ = 360° for ∼1 s); two well-resolved spots (i−ii and iv−v in Figure 3c) reveal that the endosome stays motionless for 2.5(±1.6) s. Multiple spots (3 in Figure 3c) did not show drift in their trajectory, which suggests some discontinuity within the middle of stacks (Figure S13). We interpret the discontinuity as resulting from the tilting or rotation of endosomes, rather than from deformations caused by elasticity or the development of endosomes, on the basis of differences in time scale and frequency (microseconds to milliseconds for an elastic deformation and minutes to hours for the fusion of early endosomes). Additional observations of endosomes and membrane-bound NRs under fixed polarization also show negligible fluctuations of plasmonic signal for all processes, including membrane binding, endosomal transport, and pause (Figure S5c−e), indicating that both the nature of cargo binding on MT and the inner vesicular environment are sufficiently static and rigid to allow us to disregard the trembling or diffusive behaviors of the probes. Therefore, our imaging technique can temporally separate the previously reported conventional pause (∼8 s) and pauses (SR) with subtle rotating moments (Figure 3d and Note S1). Since the quantized movements during the real pause are far from Brownian motion, we interpret that the pause of endosomes is not related to the detachment of motors—the so-called diffusive model. Instead, it is caused by the balance of their forces at the intersection, which supports the draw model at the crossroad.

To infer the three-dimensional geometry by pdf-STORM, we first let the vesicles move along the x axis (Figure 4a). Because the two SiO_2-coated NRs inside an endosome are bound to the shell and the round membrane covers the contents tightly (Figure 1d), we assumed that the two NRs are immobilized inside the lipid wall by multiple binding, that the inter-NR distance (r, Figure 1b) is maintained while d was changed, and that they are located opposite each other in the vesicle. Subsequently, the observed stacks of pdf-STORM coordinates can be converted to the axis-angle representation in a Euclidian space to define the angular displacements of an endosome. This was performed using the formula $\Phi = e(e_x, e_y, e_z) = \hat{n} \sin \varphi$, where φ is the angle and $\hat{n}$ is the unit vector of the rotation axis (Note S2). From hundreds of Euler vectors of subtle rotating movements, we observed three interesting points. (i) Rotating axes (e_x, e_y, and e_z) mainly point in equatorial directions; the vertical axis was rarely observed (Figure 4b). (ii) Probability plots for each axis component (x, y, and z axes) built for each angular displacement reveal that angular displacement along the y axis is the most dominant, while the rotational direction was irrelevant (Figure 4c). Overall, the direction of the angular displacement of vesicles during the pause followed the same direction as that in rolling on the existing MT (the track in the x axis). (iii) The size of the angle $|\varphi|$ can be best fit with two Gaussian distributions that contribute almost identically (Figure 4d and Figure S14), indicating that the displacement shows a random but heavy-tailed probability distribution in a confined environment. However, there are still limits to interpreting φ; an angular displacement ofover 90° is analyzed as 180 − φ°, and the molecular basis underlying the discrimination of the two Gaussian fits is unclear. A heavy-tailed distribution of step size is generally thought to be an efficient search behavior, as seen in movement patterns of cytosolic cargos,[24,25] phagocytic cells,[26] and foraging animals.[27,28] Our findings support notions regarding the appropriate strategy for investigating the directions of intricately organized meshes of MT tracks.

In summary, we report a simple and long-lasting DF SR imaging method using AuNRs, which can potentially be applied more generally. Using pdf-STORM, we observed the angular displacement of endosomes, confirmed the non-classical and dynamic nature of rotational movements during the tug of war, and clarified the biophysical parameters underlying material transport in live cells that have not been directly observed in previous studies of endosomal rotation.[29−31] We found that the displacement is discontinuous and y axis dominant and has a long-tail distribution. The data presented here also raise fundamental questions concerning the dynamics and collective behaviors of many individual endosomes, which confer macroscopically efficient material transport in live cells. Our findings along with the developing nanoscale live cell imaging techniques can renew the focus on biophysical investigations of material transport efficiency in living cells.

METHODS

Optical Microscopy

Total internal reflection fluorescence (TIRF) and single-molecule dark-field spectral optical microscopy were performed with an inverted microscope (Nikon, ECLIPSE Ti2-E) equipped with a perfect focus system (PFS, TI2-N-ND-P), a motorized stage (TI2-S-SE-E), a stage-top incubator with controlled temperature and CO_2 concentration (Okolab, UNO-T-H-PREMIXED), and an electron

https://doi.org/10.1021/jacsau.2c00180
JACS Au 2022, 2, 1596−1603

multiplying charge-coupled device (EM CCD, Andor, iXon Ultra 897). Super-resolution radial fluctuation (SSRF) images of microtubules were obtained by processing 100 frames of TIRF images using the super-resolution radial fluctuations (SRRF) algorithm (Andor). The dark-field images were acquired using an ellipsoidal dot mirror installed at a filter cube set and a mercury lamp (Nikon, C-HGFIE Intensilight) as a light source. The polarized dark-field images were acquired under a linear polarizer (Thorlabs, with N-BK7 windows, LPVISE50-A) equipped with a motorized rotation stage (Thorlabs, DDR25/M) connected to a DC Servo Motor Controller (KBD101). A laser (Nikon, LU-N4 Laser Unit, 488/561 wavelength) was used as a light source for TIRF microscopy. All dark-field, SRRF, and pdf-STORM images were observed under a 100× objective lens (Nikon, 1.49 NA, oil immersion, CFI SR HP Apochromat TIRF). For spectroscopy, a beam splitter, a spectroscopic detector (Andor, Newton DU-971), and a spectrometer (Andor, Shamrock 193i-A) equipped at the emission part of the microscope were used.

Development of pdf-STORM

The plasmonic properties of AuNRs exhibit an angle dependence on polarized light. To resolve two AuNRs within the diffraction limit, we fluctuated the intensity using two methods. For tethered AuNRs, the image was observed using a fixed polarizer and acquired with 200 fps because the motion of rotation was very fast. For AuNRs fixed on glass, the image was taken using a rotating polarizer. After subtraction of background signals with Fiji,[32] the temporally separated point spread function was fitted with an integrated Gaussian fit to locate their centers and the point maps were reconstructed using the ImageJ plug-in of the ThunderSTORM algorithm.[18] In the filtering process, the x and y coordinates, frame, and intensity of resolved particles were exported. When the polarizer was rotated, the traces of scattering intensity were fitted with the sine wavelet function.

Cell Lines and Specific Labeling of Au NR@Tf NPs in Live Cells

U2OS cells were cultured in a T25 flask (Corning), grown in DMEM with 10% FBS, and were passaged every 3−4 days. The cells were maintained at 37 °C and in 5% CO_2 in a humidified incubator (Binder, Model C 170). The pAcGFP1-Tubulin plasmid (PT3836-5, Clontech) was transfected into the U2OS cell line using the Neon Transfection system (Shock Conditions, cell number 2.5 × 105, plasmid 1 μg, voltage, width, and number 1,230 V, 10 ms, and 4, respectively) (MPK5000, Thermo Fisher). After transfection, the cells were plated and washed with media several times before use.

For microscopic observation, appropriate numbers of cells were plated on collagen I-coated 35 mm glass-bottom dishes (MatTek, P35G-0-10-C) to achieve 70% confluence. A 70 μm portion of the as-synthesized Au NR@Tf (0.2 nM) was added to cells, and the mixture was incubated for 20 min at 37 °C and washed five times with DMEM containing 10% FBS. Live cell images were acquired using dark-field microscopy. The image sequences were acquired at 85 Hz without delay.

Distribution of Step Angle for Endosomal Rotation

We evaluated the distributions of the endosomal step angle to describe the rotational dynamics of endosomes under the pause state. According to general formulations of free-spreading behavior, translational and angular displacements of Brownian particles show a Gaussian distribution.[33] Thus, we considered Gaussian distribution as a null model for the endosomal step angle. Despite this theoretical presumption, several direct observations have revealed that random fluctuations in some biological systems follow non-Gaussian distributions with exponential tails.[25,34,35] We used MATLAB's built-in Maximum Likelihood Estimation (MLE) algorithm for distribution fitting. We also examined the Akaike Information Criterion (AIC) and Bayesian Information Criterion (BIC) as measurements of the goodness of fit.

ASSOCIATED CONTENT

Supporting Information

The Supporting Information is available free of charge at https://pubs.acs.org/doi/10.1021/jacsau.2c00180.

Details of experimental methods, schematic of fabrication of an aluminum patterned dot mirror for the development of an inverted dark-field microscope, optical properties of gold nanorods compared with those of conventional fluorescence probes, acquisition strategies of pdf-STORM for immobilized or tethered AuNRs within the diffraction limit, preparation and characterization of transferrin-decorated gold nanorods for the clathrin-mediated endocytosis in live cells, Au NR@Tf not showing random Brownian motion inside endosomes as well as on the surface of the cell membrane, evaluation of the Thunder STORM algorithm using synthetic dark-field images, pdf-STORM showing performance comparable to electron microscopy on a 2D plane, negative control experiments for pdf-STORM conducted to show the importance of the alternating intensity fluctuation of the two AuNRs (when two NRs are parallel or when plasmonic coupling occurs, negative control experiments for pdf-STORM were conducted to show the importance of the angle dependence of the probes), spherical Au nanoparticles, Brownian motion of monovalent DNA-conjugated AuNR in tethered models, pdf-STORM resolution of tethered AuNRs, pause of an endocytic vesicle at the microtubule intersection, measurement of the subtle rotating periods by a sliding reconstruction range, and statistical model fitting for the step angle distribution of endosomes (PDF)

pdf-STORM acquisition from synthetic image sequences that simulate two immobilized Au nanorods (AVI)

pdf-STORM acquisition from synthetic image sequences that simulate two tethered Au nanorods (AVI)

Time-lapse movie of a single endocytic vesicle in a conventional dark-field microscope and the pdf-STORM sequences at pause (AVI)

AUTHOR INFORMATION

Corresponding Author

Daeha Seo − *Department of Physics and Chemistry, DGIST, Daegu 42988, Republic of Korea;* orcid.org/0000-0002-0454-1168; Email: livewire@dgist.ac.kr

Authors

Siwoo Jin − *Department of Physics and Chemistry, DGIST, Daegu 42988, Republic of Korea*

Jiseong Park − *Department of Physics and Chemistry, DGIST, Daegu 42988, Republic of Korea*

Wonhee John Lee − *Department of Physics and Chemistry, DGIST, Daegu 42988, Republic of Korea; Department of New Biology, DGIST, Daegu 42988, Republic of Korea*

Yongdeok Ahn − *Department of Physics and Chemistry, DGIST, Daegu 42988, Republic of Korea*

Youngchan Park − *Department of Physics and Chemistry, DGIST, Daegu 42988, Republic of Korea*

Minsoo Park − *Department of Physics and Chemistry, DGIST, Daegu 42988, Republic of Korea*

https://doi.org/10.1021/jacsau.2c00180
JACS Au 2022, 2, 1596−1603

Inchan Hwang − *School of Energy and Chemical Engineering, UNIST, Ulsan 44919, Republic of Korea*
Kwanyong Seo − *School of Energy and Chemical Engineering, UNIST, Ulsan 44919, Republic of Korea;* orcid.org/0000-0002-8443-7933

Complete contact information is available at: https://pubs.acs.org/10.1021/jacsau.2c00180

Notes

The authors declare no competing financial interest.

■ ACKNOWLEDGMENTS

The authors thank the CCRF of DGIST for their technical support for optical and electron microscopes. This work was supported by grants from the National Research Foundation of South Korea (NRF) funded by the Korean government (MSIT; Ministry of Science and ICT; NRF-2018R1A5A1025511 and NRF-2020R1A2C4002533) and the DGIST Program of the MSIT (21-HRHR+-02 and 21-DGRIP-01).

■ REFERENCES

(1) Teruel, M. N.; Meyer, T. Translocation and Reversible Localization of Signaling Proteins: A Dynamic Future for Signal Transduction. *Cell* **2000**, *103* (2), 181−184.
(2) Neefjes, J.; Jongsma, M. M. L.; Berlin, I. Stop or Go? Endosome Positioning in the Establishment of Compartment Architecture, Dynamics, and Function. *Trends Cell Biol.* **2017**, *27* (8), 580−594.
(3) Hirokawa, N.; Niwa, S.; Tanaka, Y. Molecular Motors in Neurons: Transport Mechanisms and Roles in Brain Function, Development, and Disease. *Neuron* **2010**, *68* (4), 610−638.
(4) Parker, F.; Peckham, M. Disease Mutations in Striated Muscle Myosins. *Biophys. Rev.* **2020**, *12* (4), 887−894.
(5) Newell-Litwa, K. A.; Horwitz, R.; Lamers, M. L. Non-Muscle Myosin II in Disease: Mechanisms and Therapeutic Opportunities. *DMM Dis. Model. Mech.* **2015**, *8* (12), 1495−1515.
(6) Hancock, W. O. Bidirectional Cargo Transport: Moving beyond Tug of War. *Nat. Rev. Mol. Cell Biol.* **2014**, *15* (9), 615−628.
(7) Huang, B.; Babcock, H.; Zhuang, X. Breaking the Diffraction Barrier: Super-Resolution Imaging of Cells. *Cell* **2010**, *143* (7), 1047−1058.
(8) Cheng, X.; Chen, K.; Dong, B.; Yang, M.; Filbrun, S. L.; Myoung, Y.; Huang, T.-X.; Gu, Y.; Wang, G.; Fang, N. Dynamin-dependent vesicle twist at the final stage of clathrin-mediated endocytosis. *Nat. Cell Biol.* **2021**, *23* (8), 859−869.
(9) Chakkarapani, S. K.; Sun, Y.; Lee, S.; Fang, N.; Kang, S. H. Three-Dimensional Orientation of Anisotropic Plasmonic Aggregates at Intracellular Nuclear Indentation Sites by Integrated Light Sheet Super-Resolution Microscopy. *ACS Nano* **2018**, *12* (5), 4156−4163.
(10) Park, Y.; Shin, S.; Jin, H.; Park, J.; Hong, Y.; Choi, J.; Jung, B.; Song, H.; Seo, D. Single-Molecule Rotation for EGFR Conformational Dynamics in Live Cells. *J. Am. Chem. Soc.* **2018**, *140* (45), 15161−15165.
(11) Huang, B.; Bates, M.; Zhuang, X. Super-Resolution Fluorescence Microscopy. *Annu. Rev. Biochem.* **2009**, *78*, 993−1016.
(12) Hell, S. W. Microscopy and Its Focal Switch. *Nat. Methods* **2009**, *6* (1), 24−32.
(13) Shafiei, F.; Wu, C.; Wu, Y.; Khanikaev, A. B.; Putzke, P.; Singh, A.; Li, X.; Shvets, G. Plasmonic nano-protractor based on polarization spectro-tomography. *Nat. Photonics* **2013**, *7* (5), 367−372.
(14) Funston, A. M.; Novo, C.; Davis, T. J.; Mulvaney, P. Plasmon Coupling of Gold Nanorods at Short Distances and in Different Geometries. *Nano Lett.* **2009**, *9* (4), 1651−1658.
(15) Zhang, Z.; Wang, L.; Wang, J.; Jiang, X.; Li, X.; Hu, Z.; Ji, Y.; Wu, X.; Chen, C. Mesoporous Silica-Coated Gold Nanorods as a Light-Mediated Multifunctional Theranostic Platform for Cancer Treatment. *Adv. Mater.* **2012**, *24* (11), 1418−1423.
(16) Milani, S.; Baldelli Bombelli, F.; Pitek, A. S.; Dawson, K. A.; Rädler, J. Reversible versus Irreversible Binding of Transferrin to Polystyrene Nanoparticles: Soft and Hard Corona. *ACS Nano* **2012**, *6* (3), 2532−2541.
(17) Ringe, E.; Langille, M. R.; Sohn, K.; Zhang, J.; Huang, J.; Mirkin, C. A.; Van Duyne, R. P.; Marks, L. D. Plasmon Length: A Universal Parameter to Describe Size Effects in Gold Nanoparticles. *J. Phys. Chem. Lett.* **2012**, *3* (11), 1479−1483.
(18) Ovesný, M.; Křížek, P.; Borkovec, J.; Švindrych, Z.; Hagen, G. M. ThunderSTORM: A Comprehensive ImageJ Plug-in for PALM and STORM Data Analysis and Super-Resolution Imaging. *Bioinformatics* **2014**, *30* (16), 2389−2390.
(19) Seo, D.; Southard, K. M.; Kim, J. W.; Lee, H. J.; Farlow, J.; Lee, J. U.; Litt, D. B.; Haas, T.; Alivisatos, A. P.; Cheon, J.; Gartner, Z. J.; Jun, Y. W. A Mechanogenetic Toolkit for Interrogating Cell Signaling in Space and Time. *Cell* **2016**, *165* (6), 1507−1518.
(20) Sönnichsen, C.; Reinhard, B. M.; Liphardt, J.; Alivisatos, A. P. A Molecular Ruler Based on Plasmon Coupling of Single Gold and Silver Nanoparticles. *Nat. Biotechnol.* **2005**, *23* (6), 741−745.
(21) Bálint, Š.; Verdeny Vilanova, I.; Sandoval Álvarez, Á.; Lakadamyali, M. Correlative Live-Cell and Superresolution Microscopy Reveals Cargo Transport Dynamics at Microtubule Intersections. *Proc. Natl. Acad. Sci. U. S. A.* **2013**, *110* (9), 3375−3380.
(22) Gao, Y.; Anthony, S. M.; Yu, Y.; Yi, Y.; Yu, Y. Cargos Rotate at Microtubule Intersections during Intracellular Trafficking. *Biophys. J.* **2018**, *114* (12), 2900−2909.
(23) Tanenbaum, M. E.; Gilbert, L. A.; Qi, L. S.; Weissman, J. S.; Vale, R. D. A Protein-Tagging System for Signal Amplification in Gene Expression and Fluorescence Imaging. *Cell* **2014**, *159* (3), 635−646.
(24) Chen, K.; Wang, B.; Granick, S. Memoryless Self-Reinforcing Directionality in Endosomal Active Transport within Living Cells. *Nat. Mater.* **2015**, *14* (6), 589−593.
(25) Wang, B.; Kuo, J.; Bae, S. C.; Granick, S. When Brownian Diffusion Is Not Gaussian. *Nat. Mater.* **2012**, *11* (6), 481−485.
(26) Harris, T. H.; Banigan, E. J.; Christian, D. A.; Konradt, C.; Wojno, E. D. T.; Norose, K.; Wilson, E. H.; John, B.; Weninger, W.; Luster, A. D.; Liu, A. J.; Hunter, C. A. Generalized Lévy Walks and the Role of Chemokines in Migration of Effector CD8 + T Cells. *Nature* **2012**, *486* (7404), 545−548.
(27) Viswanathan, G. M.; Afanasyev, V.; Buldyrev, S. V.; Murphy, E. J.; Prince, P. A.; Stanley, H. E. Lévy Flight Search Patterns of Wandering Albatrosses. *Nature* **1996**, *381* (6581), 413−415.
(28) Humphries, N. E.; Queiroz, N.; Dyer, J. R. M.; Pade, N. G.; Musyl, M. K.; Schaefer, K. M.; Fuller, D. W.; Brunnschweiler, J. M.; Doyle, T. K.; Houghton, J. D. R.; Hays, G. C.; Jones, C. S.; Noble, L. R.; Wearmouth, V. J.; Southall, E. J.; Sims, D. W. Environmental context explains Lévy and Brownian movement patterns of marine predators. *Nature* **2010**, *465* (7301), 1066−1069.
(29) Kapitein, L. C.; Schlager, M. A.; Van Der Zwan, W. A.; Wulf, P. S.; Keijzer, N.; Hoogenraad, C. C. Probing Intracellular Motor Protein Activity Using an Inducible Cargo Trafficking Assay. *Biophys. J.* **2010**, *99* (7), 2143−2152.
(30) Gu, Y.; Sun, W.; Wang, G.; Jeftinija, K.; Jeftinija, S.; Fang, N. Rotational Dynamics of Cargos at Pauses during Axonal Transport. *Nat. Commun.* **2012**, *3*, 1030.
(31) Kaplan, L.; Ierokomos, A.; Chowdary, P.; Bryant, Z.; Cui, B. Rotation of Endosomes Demonstrates Coordination of Molecular Motors during Axonal Transport. *Sci. Adv.* **2018**, *4* (3), No. e1602170.
(32) Schindelin, J.; Arganda-Carreras, I.; Frise, E.; Kaynig, V.; Longair, M.; Pietzsch, T.; Preibisch, S.; Rueden, C.; Saalfeld, S.; Schmid, B.; Tinevez, J. Y.; White, D. J.; Hartenstein, V.; Eliceiri, K.; Tomancak, P.; Cardona, A. Fiji: An Open-Source Platform for Biological-Image Analysis. *Nat. Methods* **2012**, *9* (7), 676−682.

(33) Han, Y.; Alsayed, A. M.; Nobili, M.; Zhang, J.; Lubensky, T. C.; Yodh, A. G. Brownian Motion of an Ellipsoid. *Science* **2006**, *314* (5799), 626−630.
(34) Golan, Y.; Sherman, E. Resolving Mixed Mechanisms of Protein Subdiffusion at the T Cell Plasma Membrane. *Nat. Commun.* **2017**, *8*, 15851.
(35) Witzel, P.; Götz, M.; Lanoiselée, Y.; Franosch, T.; Grebenkov, D. S.; Heinrich, D. Heterogeneities Shape Passive Intracellular Transport. *Biophys. J.* **2019**, *117* (2), 203−213.

https://doi.org/10.1021/jacsau.2c00180
JACS Au 2022, 2, 1596−1603